Pergamon

Int. J. Heat Mass Transfer. Vol. 37, No. 4, pp. 605–618, 1994

0017–9310/94 $6.00 + 0.00

The thermal boundary layer in a rotating cylinder subject to prescribed surface heat fluxes

W. Y. D. YUEN

Research and Technology Centre, BHP Steel, Sheet & Coil Products Division, P.O. Box 77, Port Kembla, NSW, 2505, Australia

(*Received* 9 *June* 1993 *and in final form* 23 *August* 1993)

Abstract—An examination is made of the temperature distribution in the thin thermal boundary layer induced in the sub-surface of a fast rotating cylinder subject to prescribed surface heat fluxes. Based on an asymptotic analysis, a series solution for the temperature field is obtained and an algorithm for the efficient computation of the series suggested. The solution has numerous advantages over those of previous studies for its simplicity and free from numerical instability and excessive demand on computing time, the latter drawbacks being typical of numerical solutions of heat transfer in advection-dominated regions. The closed-formed solution derived in this paper provides further insight into the physics of the problem and allows for parametric variations to be examined readily. This study finds applications in various industrial processes including strip rolling and grinding.

1. INTRODUCTION

MANY INDUSTRIAL processes involve a rotating cylinder subject to heating and cooling over its surface, as shown in Fig. 1. A common feature of the heating is that it spans over a very small zone, normally induced when the cylinder is in contact with another flat or cylindrical object and hence the arc of contact is usually very small (such as in flat rolling, grinding and machining). At steady-state, the rate of heat input on the cylinder surface must equal the heat extraction rate. Because of the normally high rotational speed of the cylinder, the penetration of the surface heat fluxes is extremely small and a thin thermal boundary layer, in which the temperature varies rapidly, exists in the cylinder sub-surface. Beyond the boundary layer, the temperature of the cylinder is largely uniform. The study of this thermal boundary layer is important since the maximum and minimum temperatures attained, as well as the thermal gradients in the cylinder, often influence the operating characteristics of the industrial process concerned. In addition, this information enables the thermal fatigue on the cylinder surface to be evaluated.

Because of the extreme rapid variation of the temperature in both circumferential and radial directions, especially when the heating zone is small and the rotational speed is high, it is very difficult for measurements to be made of the temperatures in the boundary layer. The only substantial experimental data reported to date appear to be those of Stevens *et al.* [1], in the context of strip rolling. Understandably, with the complexities involved in the experimental determination of the temperature field, much effort has been spent in the theoretical analyses of this problem, which may be broadly classified into two categories: numerical and analytical.

The finite difference approach has been largely used in the numerical approach. Pioneer work was conducted by Peck *et al.* [2], who used a Lagrangian formulation in which the cylinder is considered fixed with respect to the co-ordinate system, with the boundary conditions rotating with it (i.e. periodic). Only radial heat transfer was examined in this work. A two-dimensional study which accounted also for the circumferential heat flow was carried out by Parke and Baker [3], while Poplawski and Seccombe [4] reported a model taking into consideration the heat transfer in the axial direction (i.e. along the axis of the cylinder) as well. Recently, Yuen [5] examined the transient thermal variation of a rotating cylinder with both radial and axial heat flows using the method of lines [6]. With the Lagrangian formulation adopted in the above studies, an extremely fine mesh (or time increments) needs to be used to ensure numerical stability and/or to obtain details of the temperature variations, especially around the heating region (which typically spans over a few hundredths of a radian in the rolling process).

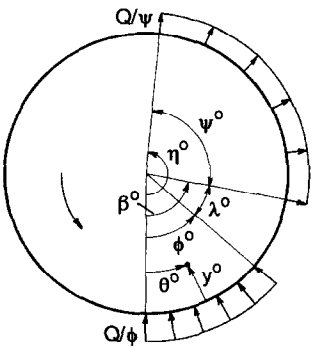

FIG. 1. Thermal system under study: rotating cylinder subject to surface heat fluxes.

NOMENCLATURE

C_{km} function related to the Binomial coefficient, defined in equation (18)
k thermal conductivity
l circumferential length of the cylinder
N limit in series summation
P Peclet number
P_ϕ $P\phi$
Q total surface heat flux per cycle in the heating zone
$T(\theta, y)$ non-dimensionalized temperature of the cylinder
$T^\circ(\theta^\circ, y^\circ)$ cylinder temperature
$T_a(\theta, y)$ non-dimensionalized temperature component: contribution from the current cycle
$T_b(\theta, y)$ non-dimensionalized temperature component: contribution from all previous cycles
T_b', T_b'' non-dimensionalized temperature component defined in equations (15)–(17)
T_m theoretical non-dimensionalized maximum temperature
$T_M(y)$ maximum non-dimensionalized temperature attained at a depth y below the cylinder surface
T_R temperature at the cylinder centre
v peripheral speed of the cylinder
y non-dimensionalized depth below the cylinder surface
y° depth below the cylinder surface
y_ϕ y/ϕ.

Greek symbols
α thermal diffusivity of the cylinder
β normalized angle defining the cooling location, Fig. 1
ζ_N function related to the Riemann zeta function, defined in equation (19)
η normalized angular position at the end of the cooling region, Fig. 1
θ normalized angular co-ordinate, $\theta^\circ/(2\pi)$
θ° angular co-ordinate
$\theta_M(y)$ normalized angular position where the temperature at a depth y below the cylinder surface reaches a maximum
λ normalized angular position of the cooling zone relative to the heating zone, Fig. 1
$\nu(\theta, y)$ normalized temperature
ϕ normalized heating zone angle, Fig. 1
ψ normalized cooling zone angle, Fig. 1.

To overcome the above difficulty, Tseng [7] suggested a first-order upwind scheme using an Eulerian formulation (in which the co-ordinate system is fixed in space such that the boundary conditions are fixed while the cylinder rotates with respect to the co-ordinate system). He demonstrated that good accuracy may be achieved with a reasonably fine mesh by this technique. Recently, Quy *et al.* [8] compared results from the finite-element analysis for the above thermal problem using four different schemes: linear elements, quadratic elements, upwind scheme and perturbation formulation. This work has also been extended to evaluate the thermal stresses in the cylinder. In addition, Chow and de Hoog [9] have used a perturbation formulation to arrive at a Fredholm integral equation of the second kind, which was then solved numerically.

On the analytical front, the separation of variables and the formulation using moving line sources have largely been used. These studies were carried out with various degrees of sophistication in the specification of the boundary conditions. Pawelski [10] employed the separation of variables technique to study the steady-state temperature of a rotating cylinder with heat flow assumed to be restricted in the radial direction only and the surface temperature taken to be prescribed (instead of prescribed heat flux). Haubitzer [11] presented an improved analysis which also included the circumferential heat flow. This work was later extended by Patula [12] who allowed for heat fluxes to be specified on the cylinder surface: a uniform heat flux in the heating region and a constant heat transfer coefficient in the convective cooling region, and by Yuen [13] who generalized the formulation to allow for any prescribed heat flux and convective heat transfer coefficient distributions over the cylinder surface. In these works, the boundary conditions are expanded in Fourier series in the circumferential direction and, hence, many terms are needed to be retained to achieve a reasonable degree of accuracy around the heating region. This invariably requires excessive computing time if details of the thermal boundary layer are to be examined [12], although substantially less terms need only be retained if the overall bulk temperature of the cylinder is sought (e.g. see Yuen [14]).

A study of the above thermal problem using the Green's function formulation of a moving heat source [15] was first reported by Cerni [16], who developed analytical expressions for the transient temperature distribution in a rotating cylinder. In his formulation, a uniform heat flux intensity in the heating region and convective cooling with a constant heat transfer coefficient over the rest of the surface have been assumed. In addition, the transient effect was computed assuming that the decrease in heat loss from the roll surface followed an exponentially decaying trend (with respect to time). A similar formulation was

adopted by Bryant and Heselton [17], who examined only the steady-state temperature but allowed for a non-uniform heat flux distribution in the heating region. By discretization, this heat flux distribution was matched with another analysis which examined the heat transfer in the body which was in contact with the rotating cylinder.

Recently, Yuen also used the moving heat source formulation to examine thermal exchanges between two semi-infinite sliding solids in contact over a finite region. The heat flux partition to each solid was determined and the resulting temperature fields in the solids evaluated. These studies, made in the context of strip rolling, considered boundary conditions where one solid had a bulk temperature different from the other [18, 19], where heat flux is generated at the contact region [20], and where heat flux is generated in the solids [21]. Asymptotic solutions based on high moving speeds (more precisely, high Peclet numbers) of the solids have been derived from these analyses. The closed-form expressions derived therein are simple and provide good accuracy without demanding excessive computing time as necessitated by some of the numerical methods discussed previously. In this paper, the technique developed in the earlier studies [18–21] is further applied to consider the thermal problem of heating/cooling of a rotating cylinder. In order to facilitate analytical solutions, only uniform heat flux intensities in the heating and cooling regions are considered here. Although this assumption somewhat simplifies the actual heating/cooling conditions as observed in most practical situations, the analysis enables simple closed-form solutions to be derived. The parametric dependence of various physical variables can be readily identified from these expressions, hence improving our understanding of the thermal process.

2. BASIC FORMULATION

Consider a cylinder rotating at a constant speed with surface heating and cooling at prescribed regions as shown in Fig. 1. When the rotational speed is high, a thin thermal boundary layer is developed on the cylinder surface at steady-state. In the analysis below, the following non-dimensionalization will be made:

(i) temperature T° by the temperature at the centre of the cylinder T°_R and the total surface heat flux per revolution Q in the heating region such that the non-dimensionalized temperature T is given by

$$T(\theta, y) = \frac{T^\circ(\theta^\circ, y^\circ) - T^\circ_R}{Q/k} \tag{1}$$

where k is the thermal conductivity of the cylinder,

(ii) the depth below the cylinder surface (in the radial direction) y° by the circumferential length l of the cylinder such that the non-dimensionalized depth y is

$$y = \frac{y^\circ}{l}, \tag{2}$$

(iii) the angular co-ordinate θ° by 2π (radians) such that the non-dimensionalized angle θ is

$$\theta = \frac{\theta^\circ}{2\pi}. \tag{3}$$

Let the periodic surface conditions be given by

$$\frac{\partial T}{\partial y}(\theta, 0) = \begin{cases} -\dfrac{1}{\phi} & \text{for } 0 < \theta < \phi \\ 0 & \text{for } \phi < \theta < \beta \\ \dfrac{1}{\psi} & \text{for } \beta < \theta < \eta \\ 0 & \text{for } \eta < \theta < 1 \end{cases} \tag{4}$$

where

$$\psi = \eta - \beta \tag{5}$$

and ϕ, β and η are non-dimensionalized angles governing the heating and cooling regions as shown in Fig. 1.

For the above boundary conditions, heating with uniform intensity (Q/ϕ) starts at $\theta = 0$ and ends at $\theta = \phi$, and heat extraction of uniform intensity (Q/ψ) starts at $\theta = \beta$ and ends at $\theta = \eta$, as shown in Fig. 1. The rest of the cylinder surface is assumed to be insulated. Note that with the boundary conditions of equations (4), the heat input equals heat extraction on the cylinder surface for each revolution (for steady-state condition). Note also that the centre temperature T°_R of the cylinder is an independent parameter (i.e. a prescribed variable).

It has been shown [22] that the non-dimensional thermal boundary layer thickness is of the order $P^{-1/2}$, where P is the Peclet number defined as

$$P = \frac{vl}{2\alpha}. \tag{6}$$

Here, v is the peripheral speed and α the thermal diffusivity of the cylinder.

In most applications, the Peclet number is high (of the order 3×10^5 to 1.5×10^6 for strip rolling) and hence the thermal boundary layer on the cylinder surface is very thin. In this boundary layer, the curvature effect becomes negligible and the above problem can be approximated by a thermal system with a semi-infinite medium in Cartesian co-ordinates (θ, y). Yuen [18] has shown, based on a Green's function formulation, that the temperature field of a semi-infinite body subject to surface heat fluxes over the region $\theta = 0$–1 is given by

$$T_a(\theta, y) = -\frac{1}{\pi}\int_0^1 \frac{\partial T}{\partial y}(\theta', 0)\, e^{P(\theta - \theta')} \times K_0\{P[(\theta - \theta')^2 + y^2]^{1/2}\}\, d\theta' \quad \text{for } 0 < \theta < 1, \tag{7}$$

where $K_0\{\ \}$ is the modified Bessel function of the second kind. With $\partial T/\partial y|_{y=0}$ of the above integral expressed by equation (4), T_a gives the cylinder tem-

perature in the thermal boundary layer induced by the surface heat fluxes of the 'current revolution'. The contribution from the previous revolutions, $T_b(\theta, y)$, may be obtained by summing their effects as follows:

$$T_b(\theta, y) = -\frac{1}{\pi}\sum_{n=1}^{\infty}\int_0^1 \frac{\partial T}{\partial y}(\theta', 0)\, e^{P(n+\theta-\theta')} \times K_0\{P[(n+\theta-\theta')^2+y^2]^{1/2}\}d\theta' \quad \text{for } 0<\theta<1 \quad (8)$$

and the overall temperature in the boundary layer at steady-state is thus given by

$$T(\theta, y) = T_a(\theta, y) + T_b(\theta, y). \quad (9)$$

3. SOLUTION

3.1. *General solution*

From the earlier results of Yuen [20], it can be shown, for $P \gg 1$, that

$$\int_{\theta_1}^{\theta_2} e^{P(\theta-\theta')}K_0\{P[(\theta-\theta')^2+y^2]^{1/2}\}\,d\theta' \approx \begin{cases} 0 & \text{for } \theta<\theta_1 \\ \pi\left\{\dfrac{2(\theta-\theta_1)}{P}\right\}^{1/2}\text{ierfc}\left\{\dfrac{Py^2}{2(\theta-\theta_1)}\right\}^{1/2} & \text{for } \theta_1<\theta<\theta_2 \\ \pi\left(\dfrac{2}{P}\right)^{1/2}\left\{(\theta-\theta_1)^{1/2}\text{ierfc}\left[\dfrac{Py^2}{2(\theta-\theta_1)}\right]^{1/2} - (\theta-\theta_2)^{1/2}\text{ierfc}\left[\dfrac{Py^2}{2(\theta-\theta_2)}\right]^{1/2}\right\} & \text{for } \theta>\theta_2 \end{cases} \quad (10)$$

where ierfc( ) is the repeated integral of the complimentary error function.

Making use of this result, the integrals in equations (7) and (8) with the boundary conditions of equations (4) may be evaluated, giving and

$$T_a(\theta, y) = \begin{cases} \dfrac{1}{\phi}\left(\dfrac{2\theta}{P}\right)^{1/2}\text{ierfc}\left[\dfrac{Py^2}{2\theta}\right]^{1/2} & \text{for } 0<\theta<\phi \\ \dfrac{1}{\phi}\left(\dfrac{2}{P}\right)^{1/2}\left\{\theta^{1/2}\text{ierfc}\left[\dfrac{Py^2}{2\theta}\right]^{1/2} - (\theta-\phi)^{1/2}\text{ierfc}\left[\dfrac{Py^2}{2(\theta-\phi)}\right]^{1/2}\right\} & \text{for } \phi<\theta<\beta \\ \dfrac{1}{\phi}\left(\dfrac{2}{P}\right)^{1/2}\left\{\theta^{1/2}\text{ierfc}\left[\dfrac{Py^2}{2\theta}\right]^{1/2} - (\theta-\phi)^{1/2}\text{ierfc}\left[\dfrac{Py^2}{2(\theta-\phi)}\right]^{1/2}\right\} - \dfrac{1}{\psi}\left[\dfrac{2(\theta-\beta)}{Py}\right]^{1/2}\text{ierfc}\left[\dfrac{Py^2}{2(\theta-\beta)}\right]^{1/2} & \text{for } \beta<\theta<\eta \\ \dfrac{1}{\phi}\left(\dfrac{2}{P}\right)^{1/2}\left\{\theta^{1/2}\text{ierfc}\left[\dfrac{Py^2}{2\theta}\right]^{1/2} - (\theta-\phi)^{1/2}\text{ierfc}\left[\dfrac{Py^2}{2(\theta-\phi)}\right]^{1/2}\right\} - \dfrac{1}{\psi}\left(\dfrac{2}{P}\right)^{1/2}\left\{(\theta-\beta)^{1/2}\text{ierfc}\left[\dfrac{Py^2}{2(\theta-\beta)}\right]^{1/2} - (\theta-\eta)^{1/2}\text{ierfc}\left[\dfrac{Py^2}{2(\theta-\eta)}\right]^{1/2}\right\} & \text{for } \eta<\theta<1 \end{cases} \quad (11)$$

Table 1. Calculated normalized temperature at selected positions based on the truncated series solution of equation (12)

		Normalized temperature, v				
		n_{max}				
$P^{1/2}y$	θ	10	100	1000	10 000	Correct values†
0	0	−0.5523	−0.5805	−0.5901	−0.5913	−0.5935
	0.1	0.7253	0.6973	0.6880	0.6834	0.6844
	0.75	0.0832	0.0565	0.0470	0.0450	0.0436
	1	−0.5543	−0.5806	−0.5901	−0.5913	−0.5935
0.1	0	−0.4107	−0.4388	−0.4482	−0.4529	−0.4518
	0.1	0.3875	0.3595	0.3502	0.3454	0.3465
	0.75	0.0828	0.0561	0.0469	0.0445	0.0431
	1	−0.4126	−0.4389	−0.4483	−0.4529	−0.4518
0.5	0	−0.0624	−0.0900	−0.0994	−0.1003	−0.1030
	0.1	−0.0546	−0.0821	−0.0917	−0.0981	−0.0951
	0.75	0.0725	0.0462	0.0366	0.0339	0.0333
	1	−0.0642	−0.0901	−0.0994	−0.1003	−0.1030

Input data used: $\phi = 0.1$, $\beta = 0.75$, $\psi = 0.25$.
† From the last column of Table 3.

$$T_b(\theta,y)=\frac{1}{\phi}\left(\frac{2}{P}\right)^{1/2}\sum_{n=1}^{\infty}\left\{(n+\theta)^{1/2}\,\mathrm{ierfc}\left[\frac{Py^2}{2(n+\theta)}\right]^{1/2}\right.$$
$$\left.-(n+\theta-\phi)^{1/2}\,\mathrm{ierfc}\left[\frac{Py^2}{2(n+\theta-\phi)}\right]^{1/2}\right\}$$
$$-\frac{1}{\psi}\left(\frac{2}{P}\right)^{1/2}\sum_{n=1}^{\infty}\left\{(n+\theta-\beta)^{1/2}\,\mathrm{ierfc}\left[\frac{Py^2}{2(n+\theta-\beta)}\right]^{1/2}\right.$$
$$\left.-(n+\theta-\eta)^{1/2}\,\mathrm{ierfc}\left[\frac{Py^2}{2(n+\theta-\eta)}\right]^{1/2}\right\}$$
$$\text{for } 0<\theta<1. \quad (12)$$

It should be noted that when $n \gg 1$, all terms higher than $O(n^{-3/2})$ in the series of the above equation cancel out with each other, and hence the series in equation (12) is bounded.

Unfortunately the series solution of equation (12) poses problems in its numerical computation since these series are very slowly convergent; an excessive number of terms needs to be retained to achieve reasonable accuracy, as illustrated in the numerical results given in Table 1. In this illustration, the non-dimensionalized temperature has been normalized, for convenience, by the 'theoretical non-dimensionalized maximum temperature', T_m, which is located on the surface of the cylinder at the end of the heating zone, thus

$$v(\theta,y)=\frac{T(\theta,y)}{T_m} \quad (13)$$

where [20]

$$T_m=\left(\frac{2}{\pi P\phi}\right)^{1/2}. \quad (14)$$

This theoretical maximum temperature T_m is one which would be reached if the contributions from the previous revolutions were neglected. It has traditionally been used in estimating the peak temperature reached in rubbing surfaces and is also known as the 'flash temperature' [23] in the context of sliding and wear.

An alternative computational scheme is adopted to overcome the above problem: the series in equation (12) is summed for the first N terms, where N is a sufficiently large number. The rest of the series is then summed after expanding each term for large n. Hence, equation (12) can be written alternatively as

$$T_b(\theta,y)=T_b'(\theta,y)+T_b''(\theta,y) \quad (15)$$

where

$$T_b'(\theta,y)=\frac{1}{\phi}\left(\frac{2}{P}\right)^{1/2}\sum_{n=1}^{N-1}\left\{(n+\theta)^{1/2}\,\mathrm{ierfc}\left[\frac{Py^2}{2(n+\theta)}\right]^{1/2}\right.$$
$$\left.-(n+\theta-\phi)^{1/2}\,\mathrm{ierfc}\left[\frac{Py^2}{2(n+\theta-\phi)}\right]^{1/2}\right\}$$
$$-\frac{1}{\psi}\left(\frac{2}{P}\right)^{1/2}\sum_{n=1}^{N-1}\left\{(n+\theta-\beta)^{1/2}\,\mathrm{ierfc}\left[\frac{Py^2}{2(n+\theta-\beta)}\right]^{1/2}\right.$$
$$\left.-(n+\theta-\eta)^{1/2}\,\mathrm{ierfc}\left[\frac{Py^2}{2(n+\theta-\eta)}\right]^{1/2}\right\}$$
$$\text{for } 0<\theta<1 \quad (16)$$

and T_b'' has the same form as T_b' (equation (16)), with the lower and upper limits in the summations replaced by N and ∞, respectively.

When N is large, the terms in the infinite series of T_b'' may be expanded for large n to give, after some mathematical manipulations:

$$T_b''(\theta,y)=\left(\frac{2}{\pi P}\right)^{1/2}\sum_{m=2}^{\infty}$$
$$\times\left\{\left(C_{0m}\zeta_N\left(m-\frac{1}{2}\right)+\frac{Py^2}{2}C_{1m}\zeta_N\left(m+\frac{1}{2}\right)\right.\right.$$
$$\left.-\frac{P^2y^4}{24}C_{2m}\zeta_N\left(m+\frac{3}{2}\right)+\frac{P^3y^6}{240}C_{3m}\zeta_N\left(m+\frac{5}{2}\right)+\ldots\right)$$
$$\left.\times\left(\frac{\theta^m-(\theta-\phi)^m}{\phi}-\frac{(\theta-\beta)^m-(\theta-\eta)^m}{\psi}\right)\right\} \quad (17)$$

where C_{km}, $k=0,1,2,\ldots$, are related to the Binomial coefficients, defined as

$$C_{km}=\binom{\frac{1}{2}-k}{m}=\frac{\Gamma(\frac{3}{2}-k)}{\Gamma(m+1)\Gamma(\frac{3}{2}-k-m)} \quad (18)$$

and

$$\zeta_N(z)=\sum_{k=N}^{\infty}k^{-z}. \quad (19)$$

Here $\Gamma(\ )$ is the Gamma function and $\zeta_N(\ )$ is related to the Riemann zeta function (ζ_1 is the Riemann zeta function). Since $\zeta_N(z)$ decreases rapidly as N and z increase, as illustrated in Table 2, relatively few terms need to be retained in equation (17) to achieve reasonable accuracy. This is illustrated in Table 3 based on the same heating/cooling conditions examined in Table 1. In these calculations, the series in equation (17) has been truncated at $m=6$ and terms higher than $O(P^3y^6)$ have been neglected. It can be seen that excellent accuracy is achieved, even for N as small as 4.

The merit of this alternative scheme is best demonstrated in a comparison of the computational times between the two methods of solution, as shown in Table 4. Clearly, the more efficient scheme using equations (15)–(17) requires much smaller computational times, yet producing more accurate results. In addition, the timings using a previous series solution [13] are also included in the table. It was noted in that work [13] that at least 500 terms needed to be retained in order to achieve a 1% solution accuracy. These comparisons clearly illustrated the superiority of the alternative computational scheme.

Table 2. Illustrative values of the function $\zeta_N(z)$

z	$\zeta_N(z)$ $N=4$	$N=20$	$N=100$	$N=200$
1.5	1.0664	0.4529	0.2005	0.1416
2.5	0.1006	7.7389×10^{-3}	6.7169×10^{-4}	2.3659×10^{-4}
3.5	1.6962×10^{-2}	2.3799×10^{-4}	4.0503×10^{-6}	7.1154×10^{-7}
4.5	3.3856×10^{-3}	8.7109×10^{-6}	2.9075×10^{-8}	2.5476×10^{-9}
5.5	7.3157×10^{-4}	3.4710×10^{-7}	2.2727×10^{-10}	—
6.5	1.6538×10^{-4}	1.4546×10^{-8}	—	—
7.5	3.8464×10^{-5}	6.3030×10^{-10}	—	—
8.5	9.1177×10^{-6}	†	—	—

† All results smaller than 10^{-10} are omitted.

Table 3. Calculated normalized temperature at selected positions based on the alternative computational scheme (equations (15)–(17))

$P^{1/2}y$	θ	Normalized temperature, v $N=4$	$N=20$	$N=100$	$N=200$
0	0	−0.5935	−0.5935	−0.5935	−0.5935
	0.1	0.6843	0.6843	0.6843	0.6844
	0.75	0.0435	0.0435	0.0435	0.0436
	1	−0.5935	−0.5935	−0.5935	−0.5935
0.1	0	−0.4518	−0.4519	−0.4519	−0.4518
	0.1	0.3465	0.3465	0.3465	0.3465
	0.75	0.0431	0.0431	0.0431	0.0431
	1	−0.4519	−0.4518	−0.4519	−0.4518
0.5	0	−0.1030	−0.1030	−0.1031	−0.1030
	0.1	−0.0951	−0.0951	−0.0951	−0.0951
	0.75	0.0332	0.0332	0.0332	0.0333
	1	−0.1030	−0.1030	−0.1031	−0.1030

Input data: $\phi = 0.1$, $\beta = 0.75$, $\psi = 0.25$.

3.2. *Surface temperatures*

Of special interest is the surface temperature of the cylinder where rapid thermal variations occur. This surface temperature distribution has important implications in practical applications since it could affect, for instance, the lubricant characteristics (in the case of the rolling and grinding processes) and the convective heat extraction rate. By setting $y = 0$ to the previous results, simple expressions for the surface temperatures can be obtained:

$$T_a(\theta,0) = \begin{cases} \dfrac{1}{\phi}\left(\dfrac{2\theta}{\pi P}\right)^{1/2} & \text{for } 0<\theta<\phi \\ \dfrac{1}{\phi}\left(\dfrac{2}{\pi P}\right)^{1/2}\{\theta^{1/2}-(\theta-\phi)^{1/2}\} & \text{for } \phi<\theta<\beta \\ \dfrac{1}{\phi}\left(\dfrac{2}{\pi P}\right)^{1/2}\{\theta^{1/2}-(\theta-\phi)^{1/2}\}-\dfrac{1}{\psi}\left(\dfrac{2}{\pi P}\right)^{1/2}(\theta-\beta)^{1/2} & \text{for } \beta<\theta<\eta \\ \dfrac{1}{\phi}\left(\dfrac{2}{\pi P}\right)^{1/2}\{\theta^{1/2}-(\theta-\phi)^{1/2}\} & \\ \quad -\dfrac{1}{\psi}\left(\dfrac{2}{\pi P}\right)^{1/2}\{(\theta-\beta)^{1/2}-(\theta-\eta)^{1/2}\} & \text{for } \eta<\theta<1 \end{cases} \tag{20}$$

and

$$T_b(\theta,0) = \left(\frac{2}{\pi P}\right)^{1/2}\sum_{n=1}^{\infty}\left\{\frac{1}{\phi}[(n+\theta)^{1/2}-(n+\theta-\phi)^{1/2}]\right.$$

Table 4. Comparison of the computational times for the results given in Tables 1 and 3, and for those using a previous series solution [13]

		Computational time
Table 1:	$n_{max} = 10$	1.8
	100	17
	1000	173
	10000	1730
Table 3:	$N = 4$†	1.0
	20	3.8
	100	18
	200	35
Ref. [13]:	$n = 50$‡	15
	100	86
	200	602
	500	8680

† Reference.

‡ n is the number of terms retained in the series solution.

$$-\frac{1}{\psi}[(n+\theta-\beta)^{1/2}-(n+\theta-\eta)^{1/2}]\Bigg\}$$

for $0<\theta<1$. (21)

Again, for efficient numerical computation, $T_b(\theta,0)$ may be written as a sum of $T_b'(\theta,0)$ and $T_b''(\theta,0)$ where

$$T_b'(\theta,0)=\left(\frac{2}{\pi P}\right)^{1/2}\sum_{n=1}^{N-1}\left\{\frac{1}{\phi}[(n+\theta)^{1/2}-(n+\theta-\phi)^{1/2}]\right.$$
$$\left.-\frac{1}{\psi}[(n+\theta-\beta)^{1/2}-(n+\theta-\eta)^{1/2}]\right\}$$

for $0<\theta<1$ (22)

and

$$T_b''(\theta,0)=\left(\frac{2}{\pi P}\right)^{1/2}\sum_{m=2}^{\infty}\left\{\left[C_{0m}\zeta_N\left(m-\frac{1}{2}\right)\right]\right.$$
$$\left.\times\left[\frac{\theta^m-(\theta-\phi)^m}{\phi}-\frac{(\theta-\beta)^m-(\theta-\eta)^m}{\psi}\right]\right\}$$

for $0<\theta<1$. (23)

Here, C_{0m} and $\zeta_N()$ are given by equations (18) and (19), respectively.

3.3. *Special case of line heat source/sink*

Another case of interest is when the heating and cooling regions are small (compared to the circumferential area of the cylinder) such that the heat fluxes can be considered as line sources. In this case, $\phi\to 0$ and $\psi\to 0$. It can be shown that the temperature field of the cylinder is then given by

$$T_a(\theta,y)=\begin{cases}\dfrac{\exp\{-Py^2/(2\theta)\}}{(2\pi P\theta)^{1/2}} & \text{for } 0<\theta<\beta\\[2ex] \dfrac{\exp\{-Py^2/(2\theta)\}}{(2\pi P\theta)^{1/2}}-\dfrac{\exp\{-Py^2/[2(\theta-\beta)]\}}{\{2\pi P(\theta-\beta)\}^{1/2}} & \text{for } \beta<\theta<1\end{cases}$$ (24)

$$T_b(\theta,y)=\left(\frac{1}{2\pi P}\right)^{1/2}\sum_{n=1}^{\infty}\left\{\frac{\exp\{-Py^2/[2(n+\theta)]\}}{(n+\theta)^{1/2}}\right.$$
$$\left.-\frac{\exp\{-Py^2/[2(n+\theta-\beta)]\}}{(n+\theta-\beta)^{1/2}}\right\}\quad\text{for } 0<\theta<1.\quad(25)$$

Again, for computational purpose, T_b may be evaluated by summing to $N-1$ terms (T_b') with the remainder (T_b'') summed, after a suitable expansion:

$$T_b''(\theta,y)=\left(\frac{1}{2\pi P}\right)^{1/2}\sum_{m=1}^{\infty}\left\{\left[C_{1m}\zeta_N\left(m+\frac{1}{2}\right)\right.\right.$$
$$-\frac{Py^2}{2}C_{2m}\zeta_N\left(m+\frac{3}{2}\right)+\frac{P^2y^4}{8}C_{3m}\zeta_N\left(m+\frac{5}{2}\right)$$
$$\left.\left.-\frac{P^3y^6}{48}C_{4m}\zeta_N\left(m+\frac{7}{2}\right)+\ldots\right][\theta^m-(\theta-\beta)^m]\right\}$$

for $0<\theta<1$. (26)

Note that the surface temperature in this case is

$$T_a(\theta,0)=\begin{cases}\left[\dfrac{1}{2\pi P\theta}\right]^{1/2} & \text{for } 0<\theta<\beta\\[2ex] \left[\dfrac{1}{2\pi P\theta}\right]^{1/2}-\left[\dfrac{1}{2\pi P(\theta-\beta)}\right]^{1/2} & \text{for } \beta<\theta<1\end{cases}$$ (27)

$$T_b(\theta,0)=\left(\frac{1}{2\pi P}\right)^{1/2}\sum_{n=1}^{\infty}\left\{\left[\frac{1}{n+\theta}\right]^{1/2}\right.$$
$$\left.-\left[\frac{1}{(n+\theta-\beta)}\right]^{1/2}\right\}\quad\text{for } 0<\theta<1.\quad(28)$$

Hence, the surface temperatures tend to ∞ and $-\infty$, respectively, at the heating and cooling locations ($\theta=0$ and β). However, the temperatures are finite below the cylinder surface at these angular locations.

4. NUMERICAL RESULTS

Some numerical results based on the above solutions are discussed below. In all computations, N has been taken to be 20 and $m=6$ with terms up to $O(P^3y^6)$ retained.

4.1. *Individual contribution of T_a and T_b*

Figures 2(a) and (b) illustrate the contribution to the overall temperature from the surface heat fluxes during the current revolution and from all past revolutions, respectively; the combined effect is shown in Fig. 2(c). In these illustrations, the cooling is applied at the end of a cycle ($\beta=0.75$ and $\psi=0.25$), which is immediately followed by heating (since heating is assumed to be applied at the beginning of each cycle).

It can be seen from Fig. 2(a) that the thermal exchanges on the cylinder surface contributed from the current revolution induce rapid variation of the temperature on the cylinder surface, but the large thermal variation does not extend much into the cylinder subsurface. The surface temperature increases rapidly in the heating zone ($0<\theta<\phi$), decreases exponentially between the end of the heating zone and the start of the cooling zone ($\phi<\theta<\beta$) due to the inward diffusion of the thermal energy driven by the thermal gradient in the radial direction which is built up in the heating region, and decreases further in the cooling zone ($\beta<\theta<\eta$). At the end of the cooling zone, the normalized surface temperature becomes negative (i.e. below the centre temperature).

On the other hand, the surface heat fluxes of the past revolutions have a less dramatic effect on the surface temperature, as shown in Fig. 2(b). The major effect is at the start of each cycle (when θ is small) where the temperature is low; this is caused by the cooling zone from the previous revolution (which just precedes the heating zone in this illustration) inducing a chilling effect at $\theta=0$.

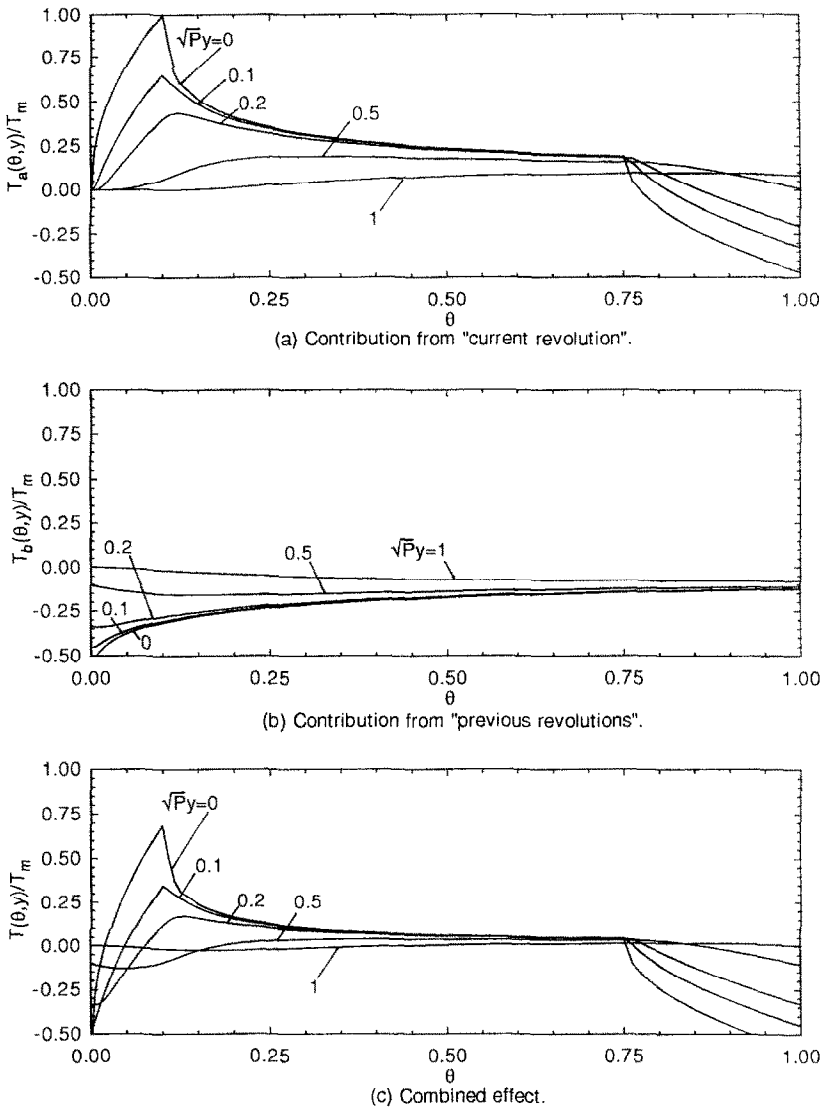

FIG. 2. Temperature distribution in the rotating cylinder ($\phi = 0.1$, $\beta = 0.75$, $\psi = 0.25$).

The combined effect of the above two factors, as shown in Fig. 2(c), produces a temperature distribution primarily governed by the first factor, except that the temperatures in the heating zone are substantially reduced. Note also that the maximum surface temperature occurs at the end of the heating zone ($\theta = \phi$). However, below the surface, the maximum temperatures occur at locations beyond the heating zone owing to the inward thermal diffusion from the surface.

4.2. *Effect of cooling location and contact angle*

Figure 3(a) illustrates the surface temperature variation with varying location angles β of the cooling zone. It can be seen that a cusp is formed at the end of the cooling zone: this is caused by the reverse thermal diffusion (from the sub-surface back to the surface) after cooling is completed. When cooling is located at the end of the cycle, the cusp disappears since it then merges into the heating zone. The peak surface temperatures (at $\theta = \phi$) and the minimum temperatures (at $\theta = \eta$) do not change appreciably as β varies: both the maximum and minimum temperatures decrease slightly as β increases.

Figure 3(b) illustrates the effect of varying the cooling contact angle ψ. The cusp becomes less pronounced as the contact angle increases; however, the maximum and minimum temperatures attained are fairly much unchanged.

It was mentioned in Section 3.1 that the temperature T_m (equation (14)) has been traditionally used to estimate the peak temperature attained in rubbing surfaces (such as grinding, rolling, etc). This temperature is obtained by neglecting the contributions from the previous revolutions, i.e. the surface heating is assumed to apply only in the region

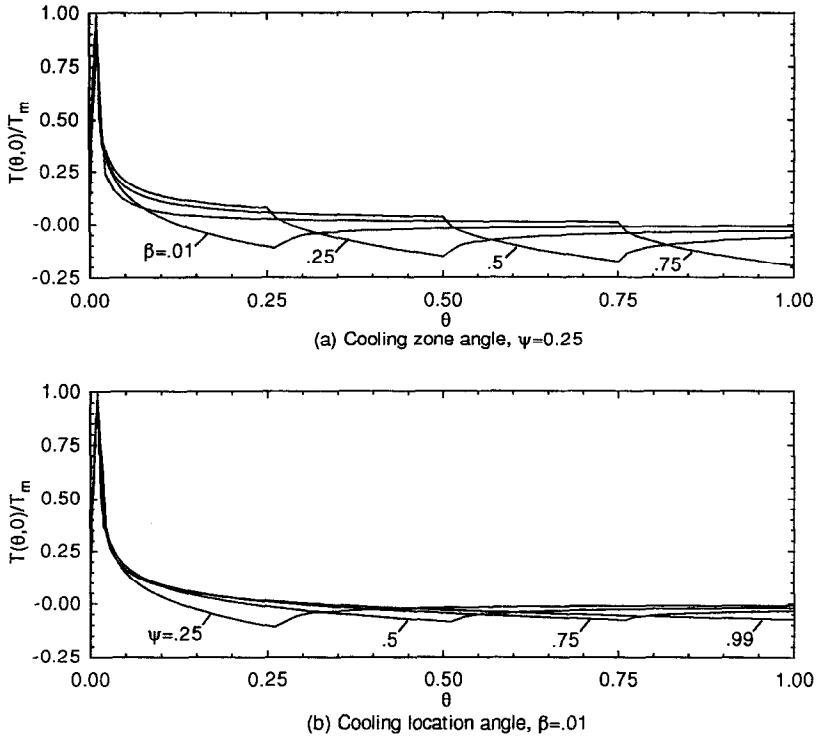

FIG. 3. Effect of the location and contact angles of the cooling zone on the surface temperature of the cylinder ($\phi = 0.01$).

$0 < \theta < \phi$ and the surface is fully insulated elsewhere ($\theta < 0$ and $\theta > \phi$). For periodic surface heat fluxes, this peak temperature could be substantially reduced under certain cooling configurations such that the normalized peak temperature $v(\phi, 0)$ is less than unity as indicated in Fig. 2(c). This effect is examined in Fig. 4 where $v(\phi, 0)$ is plotted against the heating angle ϕ for various cooling locations relative to the heating zone ($\lambda = \beta - \phi$) and contact angle ψ. It can be seen that $v(\phi, 0)$ decreases as ϕ increases, as the cooling contact angle ψ increases, and as the cooling zone is positioned further away from the heating zone. In fact, a reduction of 40–50% of the peak temperature can be experienced with certain cooling configurations, as illustrated in Fig. 4. Hence, it is important to take into consideration the effect of the periodic surface heat fluxes when predicting the peak temperature attained in the cylinder if an over-estimation is to be avoided.

4.3. *Maximum and minimum temperatures*

In the previous illustrations, the cylinder temperatures have been plotted in a normalized variable v, the normalizing parameter T_m is given in equation (14). It can be seen from that equation that T_m varies with the heating angle ϕ. In order to illustrate the variation of the actual cylinder temperature with the heating and cooling locations while keeping the total

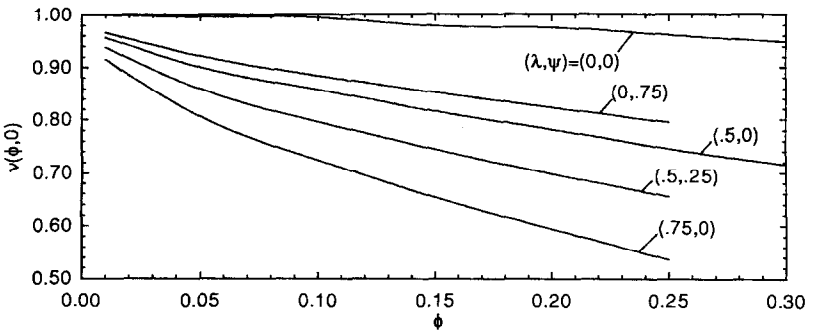

FIG. 4. Effect of the heating and cooling location and contact angles on the peak temperature reached on the cylinder surface ($\lambda = \beta - \phi$).

heat fluxes per revolution Q constant, a more appropriate parameter $v/\phi^{1/2}$ should be adopted since

$$\frac{v(0,y)}{\phi^{1/2}} \equiv \frac{T(0,y)}{T_m\phi^{1/2}} = \left(\frac{1}{2}\pi P\right)^{1/2}\left[\frac{k(T^\circ - T_R^\circ)}{Q^\circ}\right] \quad (29)$$

which is independent of ϕ.

Of interest are the maximum and minimum temperatures in the cylinder, which are both located on the surface, the former at the end of the heating zone (i.e. $T(\phi,0)$) and the latter at the end of the cooling zone (i.e. $T(\eta,0)$). These temperatures have important implications on the change in metallurgical properties in the cylinder sub-surface (if the maximum temperature is excessively high), the lubricant performance, the surface heat extraction rate (for convective cooling) and the thermal fatigue. In addition, the high thermal gradient, which generally occurs across the heating region (since ϕ is normally small compared to the cooling contact angle ψ), is also of interest since it provides an estimate of the thermal shock on the cylinder surface, which is indicated by the overall temperature jump across the heating zone ($T(\phi,0) - T(0,0)$). The effects of variation in the heating/cooling angles on these temperatures are illustrated in Fig. 5. It can be seen, from Fig. 5(a), that the heating angle ϕ largely governs the peak temperature: the smaller the heating angle, the higher is the peak temperature. The effect of the cooling locations (λ and ψ) is relatively insignificant. On the other hand, the cooling contact angle ψ has a significant effect on the minimum temperature as shown in Fig. 5(b): the smaller the contact angle, the lower is the minimum tem-

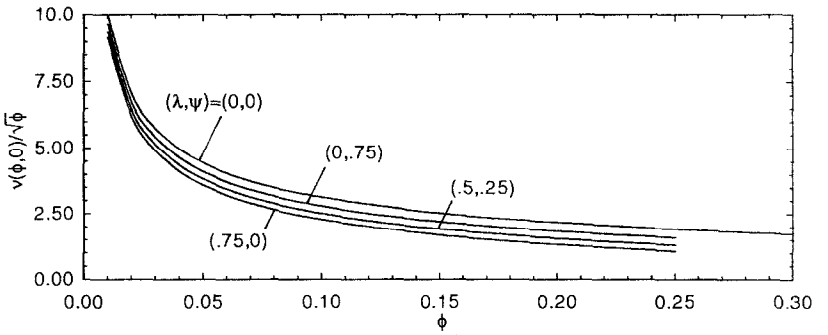

(a) Maximum temperature (at the end of the heating zone).

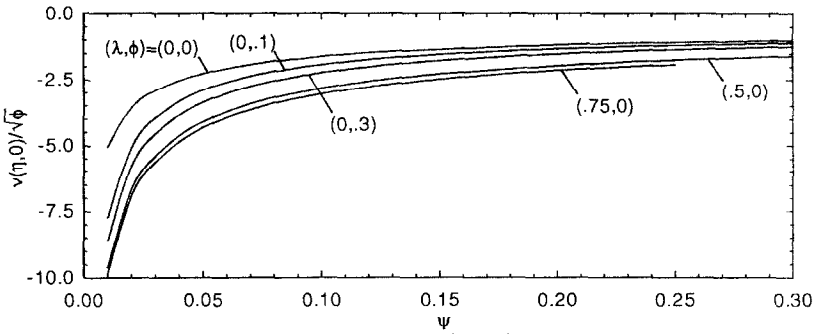

(b) Minimum temperature (at the end of the cooling zone).

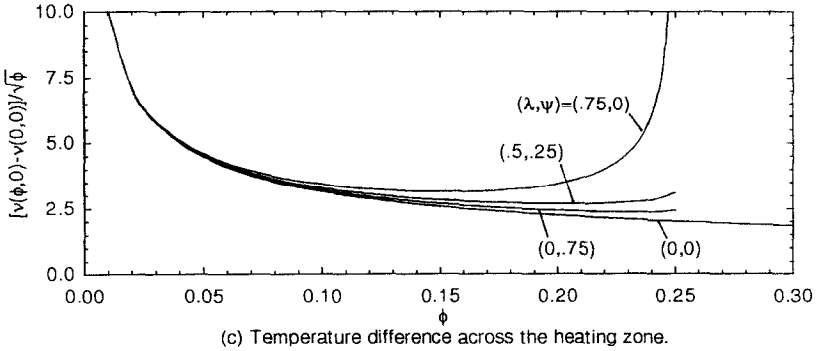

(c) Temperature difference across the heating zone.

FIG. 5. Variation of the cylinder temperature at selected surface locations with the heating and cooling configuration.

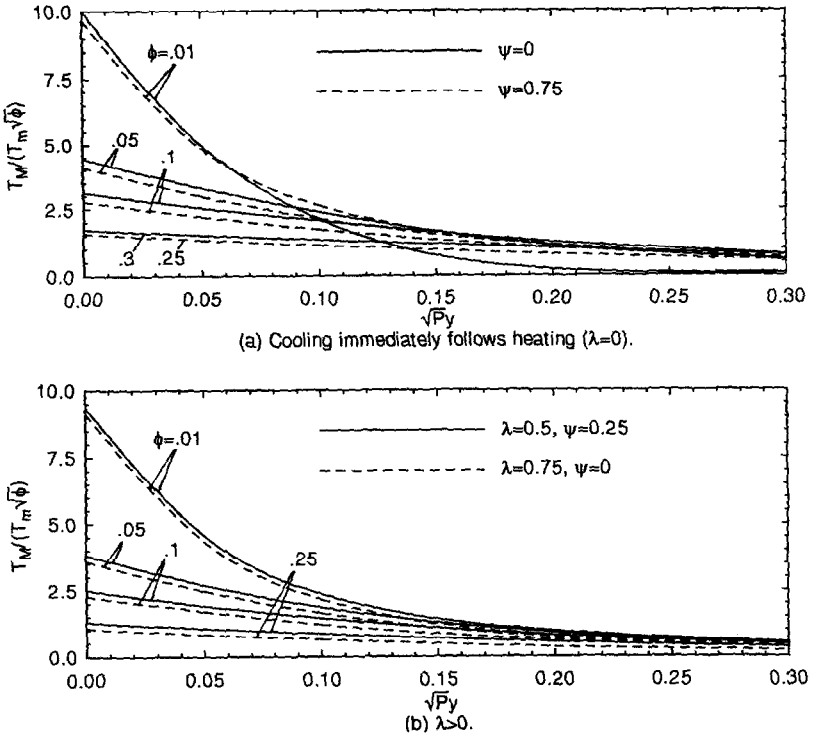

FIG. 6. Thermal penetration below the cylinder surface.

perature. In addition, the minimum temperature tends to be higher when cooling follows heating immediately ($\lambda = 0$). In this situation, the heating angle ϕ has a moderate effect when the cooling contact angle is small. Otherwise the effect of ϕ on the minimum temperature is generally insignificant. Again, the heating angle ϕ is a governing factor on the temperature jump across the heating zone as shown in Fig. 5(c). The

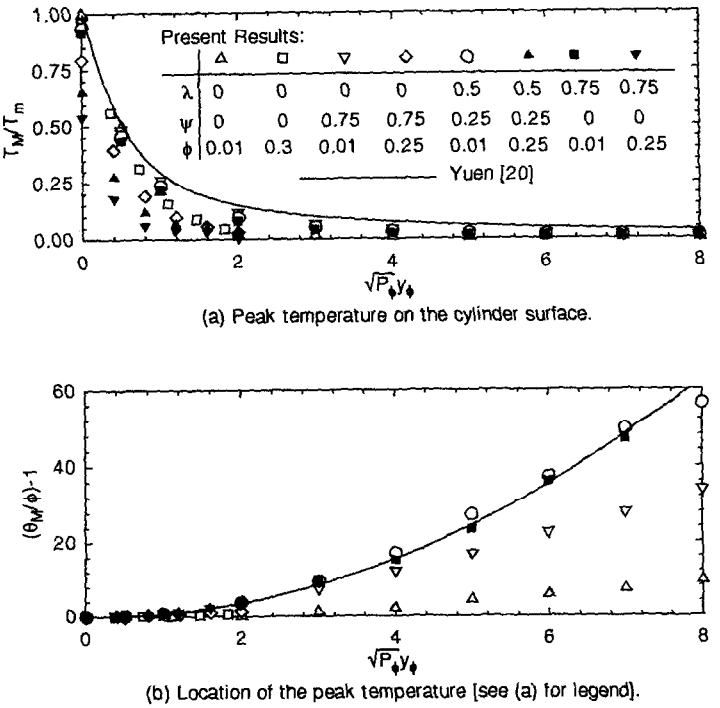

FIG. 7. Comparison of the results from the present analysis with those from a single-cycle analysis [20] for the peak temperature and its location on the cylinder.

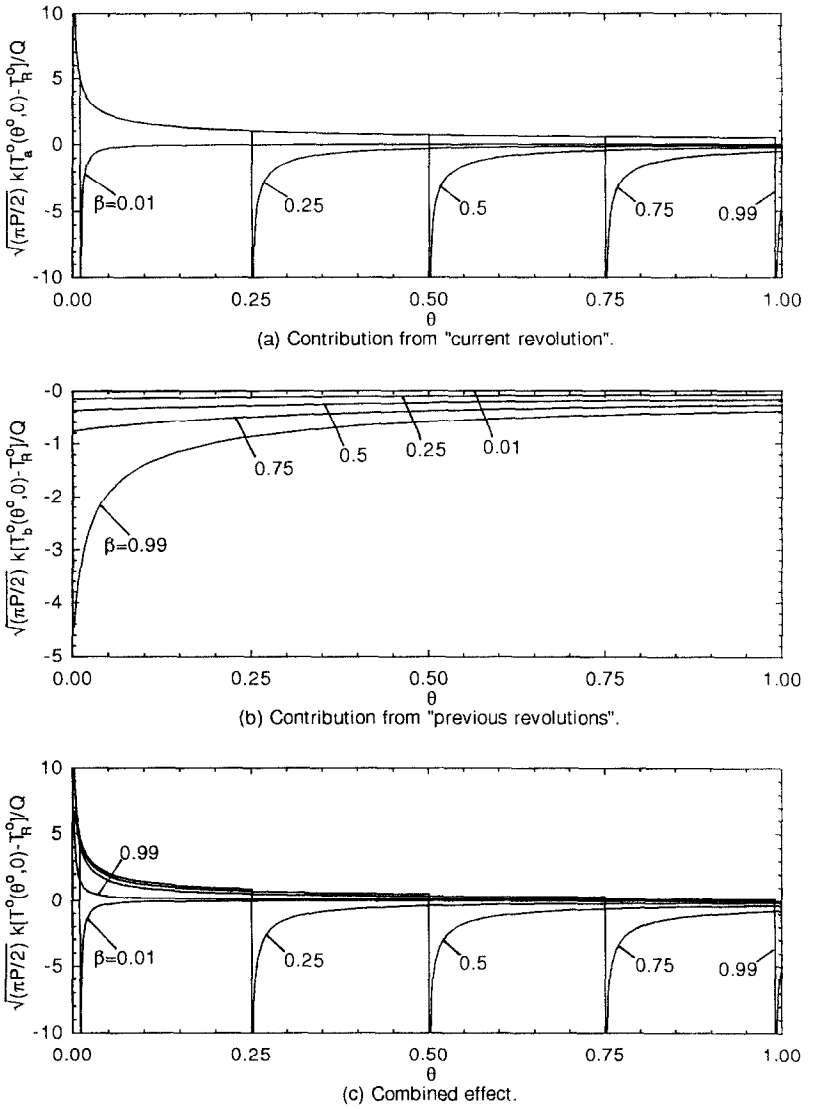

FIG. 8. Surface temperature on the cylinder based on line heat sources (both heating and cooling).

cooling locations (λ and ψ) do not have much effect except for the case when cooling just precedes heating with a small cooling contact angle ($\phi > 0.2$, $\lambda = 0.75$ and $\psi = 0$). In these circumstances, the intense cooling induces a low cylinder temperature prior to heating, hence increasing the temperature jump across the heating zone.

4.4. *Thermal penetration*

Another parameter of interest is the maximum temperature $T_M(y)$ attained at a given depth below the cylinder surface. This parameter provides a quantification of the thermal penetration into the cylinder and, in the case of strip rolling, allows the extent of thermal damages ('fire cracks') to be estimated. The variation of this temperature with $P^{1/2}y$ is shown in Fig. 6 for various heating angles ϕ, with the effect of the location of the cooling zone relative to the heating zone (λ) illustrated. It can be seen that, again, the maximum temperature T_M decreases rapidly with increasing heating angle, especially near the cylinder surface ($P^{1/2}y \leqslant 0.1$); and decreases with increasing depth into the cylinder, especially for small heating angles. The location of the cooling zone and the cooling contact angle do not have a significant effect on T_M (Fig. 6(b)) except when cooling immediately follows heating ($\lambda = 0$) with small heating and cooling angles, the effect then becomes significant (Fig. 6(a)): for $\phi = 0.01$ and $\psi = 0$, the surface tends to be hotter (at $P^{1/2}y = 0$) while the thermal penetration is less significant such that $T_M/(T_m\phi^{1/2})$ is smaller (at $P^{1/2}y$ greater than around 0.1) with respect to cases where $\phi > 0.01$ or $\psi = 0.75$. This observation has important implications in a cooling system design: different stra-

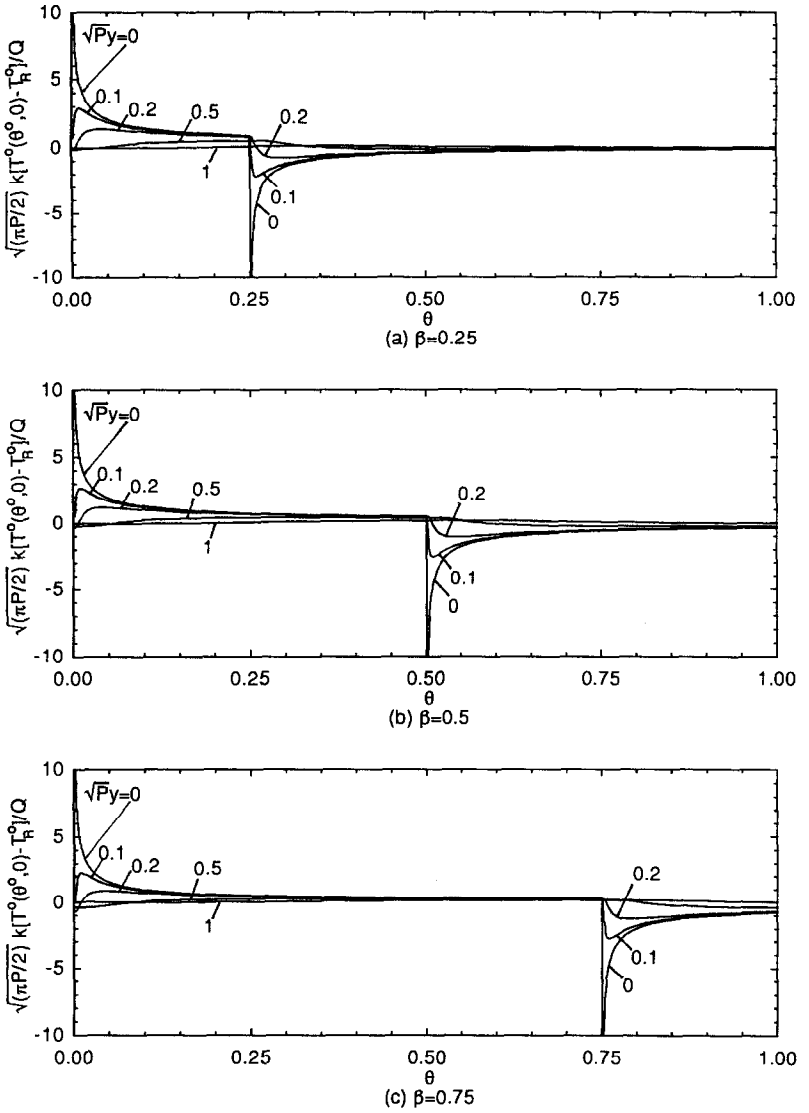

FIG. 9. Temperature distribution in the cylinder based on line heat sources (both heating and cooling).

tegies need to be adopted if one prefers to minimize the thermal penetration rather than the maximum temperature.

In a previous analysis [20] where only heating of one cycle is considered, the normalized temperature $T_M(y)/T_m$ was shown to correlate with the parameter $P_\phi^{1/2} y_\phi$, where P_ϕ and y_ϕ are the Peclet number and dimension based on the size of the heating zone ($P_\phi = \frac{1}{2}vl\phi/\alpha$, $y_\phi = y^\circ/(l\phi)$). On plotting the results of Fig. 6 in these terms (only selected curves are plotted), together with the result of the previous analysis [20], as shown in Fig. 7(a), it can be seen that the heating and cooling locations and contact angles could influence T_M substantially for the case of periodic heat fluxes. The maximum temperatures in the cylinder could be grossly over-estimated if the heating/cooling configurations and periodic heating effects are neglected in the analysis. The angular location θ_M at which these maximum temperatures occur is plotted in Fig. 7(b). It is found, again, that θ_M depends also on the heating/cooling configurations.

4.5. *Line heat sources*

Figure 8 illustrates the surface temperature of the cylinder when heating and cooling span over a very small zone such that they can be considered as line sources. In these illustrations, the parameter $(\frac{1}{2}\pi P)^{1/2}k(T^\circ - T_R^\circ)/Q$, which is equivalent to $T/(T_m\phi^{1/2})$ adopted previously, is plotted (note here that T_m is infinite). Figure 8(a) gives the contribution of the heating/cooling from the current revolution, while Fig. 8(b) gives the effect of heat sources in all past revolutions and Fig. 8(c) illustrates the combined effect. It can be seen that the temperature decreases rapidly after the heating zone ($\theta = 0$), then drops further during cooling, thereafter increases rapidly

again to reach a temperature close to the cylinder centre temperature. It is noted that these temperature variations are in the form of $\theta^{-1/2}$ (see, for example, equation (24) with $y = 0$). On the other hand, the contribution from the past revolutions is most pronounced when the cooling zone is close to the end of the cycle (e.g. $\beta = 0.99$ in Fig. 8(b)). In this case, the temperature component at small θ is below the cylinder centre temperature. This in turn produces a lower overall temperature at small θ, as shown in Fig. 8(c). From this last figure, it can be seen that, apart from the case where cooling is close to the beginning or the end of the heating zone, the temperature variations just after heating and just after cooling are largely independent of β. Hence, the heating and cooling effects appear not to interact much with each other provided that they are sufficiently far apart.

The temperature distribution at various depths below the cylinder surface is shown in Fig. 9 for various values of β. It can be seen that an earlier application of cooling after the heating zone results in a marginally smaller penetration of the cooling effect into the cylinder ($\beta = 0.25$, cf. $\beta = 0.75$). The same observation can be made for heating after cooling: the penetration of the heating effect for $\beta = 0.75$ is marginally smaller than that for $\beta = 0.25$.

5. CONCLUSION

The thermal boundary layer in the subsurface of a rotating cylinder subject to surface heat fluxes is examined in this paper. Based on an asymptotic analysis, a series solution for the temperature field is derived for large Peclet numbers. A further expansion of the series solution results in a form which converges rapidly and hence offers an extremely efficient scheme for computation. This study provides a much improved analysis of the problem at hand over previous numerical or series solutions, in which numerical instability and/or slow convergence are typical for advection-dominated heat transfer problem with localized heat fluxes. This work finds applications in strip rolling, grinding and other related industrial processes.

Acknowledgement—The author wishes to thank the management of BHP Steel, Sheet and Coil Products Division, for permission to publish the information contained in this paper.

REFERENCES

1. P. G. Stevens, K. P. Ivens and P. Harper, Increasing work-roll life by improved roll-cooling practice, *J. Iron Steel Inst.* **209,** 1–11 (1971).
2. C. F. Peck, J. M. Bonetti and F. T. Mavis, Temperature stresses in iron work rolls, *Iron Steel Engr Year Book*, pp. 389–401 (1954).
3. D. M. Parke and J. L. L. Baker, Temperature effects of cooling work rolls, *Iron Steel Engr* **49**(12), 83–88 (1972).
4. J. V. Poplawski and D. A. Seccombe, Jr., Mathematical modeling system for cold tandem rolling mills: roll and strip thermal considerations. In *Science and Technology of Flat Rolled Products*, Vol. 1, pp. 611–622 (1980).
5. W. Y. D. Yuen, On the correction of strip shape by localized cooling of the work rolls, *Proc. 4th Int. Steel Rolling Conf.*, Vol. 2, pp. E.23.1–E.23.12 (1987).
6. N. K. Madsen and R. F. Sincovec, The numerical method of lines for the solution of nonlinear partial differential equations. In *Computational Methods in Nonlinear Mechanics*, pp. 371–380 (1974).
7. A. A. Tseng, A finite-difference thermal model of flat rolling. In *Numerical Methods in Industrial Forming Processes*, pp. 767–776 (1982).
8. N. V. Quy, N. E. Thompson and W. Y. D. Yuen, Evaluation of temperature and thermal stress distributions in a work roll using the finite-element method, *Proc. Rolling Technology Conf.*, pp. 142–147 (1986).
9. Y. M. Chow and F. R. de Hoog, Unpublished work.
10. O. Pawelski, Calculation of temperature field in work rolls, *Arch Eisenh* **42,** 864–869 (1971).
11. W. Haubitzer, The steady-state temperature distribution in rolls, *Arch Eisenh* **46,** 635–638 (1975).
12. E. J. Patula, Steady-state temperature distribution in a rotating roll subject to surface heat fluxes and convective cooling, *ASME J. Heat Transfer* **103,** 36–41 (1981).
13. W. Y. D. Yuen, On the steady-state temperature distribution in a rotating cylinder subject to heating and cooling over its surface, *ASME J. Heat Transfer* **106,** 578–585 (1984).
14. W. Y. D. Yuen, Effective cooling of work rolls in strip rolling, *Mater. Sci. Technol.* **4,** 628–634 (1988).
15. J. C. Jaeger, Moving sources of heat and the temperature at sliding contacts, *J. Proc. R. Soc. NSW* **76,** 203–224 (1942).
16. S. Cerni, The temperatures and thermal stresses in the rolling of metal strip, Ph.D. Thesis, Carnegie Inst. of Tech. (1961).
17. G. F. Bryant and M. O. Heselton, Roll-gap temperature models for hot mills, *Metals Technol.* **9,** 469–477 (1982).
18. W. Y. D. Yuen, A new formulation of heat transfer between two moving bodies in contact over a finite region with different bulk temperatures, *Math. Engng Ind.* **1,** 1–19 (1987).
19. W. Y. D. Yuen, Temperature fields of moving bodies with different bulk temperatures in contact over a fixed region, *Math. Engng Ind.* **1,** 215–234 (1987).
20. W. Y. D. Yuen, Heat conduction in sliding solids, *Int. J. Heat Mass Transfer* **31,** 637–646 (1988).
21. W. Y. D. Yuen, Temperature fields in sliding solids with internal heat sources, *Int. J. Heat Mass Transfer* **36,** 3711–3722 (1993).
22. W. Y. D. Yuen, On the heat transfer of a moving composite strip compressed by two rotating cylinders, *ASME J. Heat Transfer* **107,** 541–548 (1985).
23. H. Blok, The flash temperature concept, *Wear* **6,** 483–494 (1963).